IEEE Access
Multidisciplinary | Rapid Review | Open Access Journal

Received 10 February 2024, accepted 21 February 2024, date of publication 27 February 2024, date of current version 5 March 2024.

Digital Object Identifier 10.1109/ACCESS.2024.3371027

RESEARCH ARTICLE

A Miniaturized Metamaterial-Based Dual-Band 4×4 Butler Matrix With Enhanced Frequency Ratio for Sub-6 GHz 5G Applications

ABDULKADIR BELLO SHALLAH[1,2], (Member, IEEE), FARID ZUBIR[1,3], (Member, IEEE), MOHAMAD KAMAL A. RAHIM[3], (Senior Member, IEEE), NOORLINDAWATY MD. JIZAT[4], (Member, IEEE), ABDUL BASIT[5,6], MAHER ASSAAD[7], AND HUDA A. MAJID[8], (Member, IEEE)

[1]Wireless Communication Centre, Faculty of Electrical Engineering, Universiti Teknologi Malaysia, Johor Bahru, Johor 81310, Malaysia
[2]Department of Electrical and Electronics Engineering, Kebbi State University of Science and Technology, Aliero 1144, Nigeria
[3]Department of Communication Engineering, Faculty of Electrical Engineering, Universiti Teknologi Malaysia, Johor Bahru, Johor 81310, Malaysia
[4]Faculty of Engineering, Multimedia University, Cyberjaya, Selangor 63100, Malaysia
[5]School of Information Science and Engineering, NingboTech University, Ningbo 315100, China
[6]College of Information Science and Electronic Engineering, Zhejiang University, Hangzhou 310027, China
[7]Department of Electrical and Computer Engineering, College of Engineering and Information Technology, Ajman University, Ajman, United Arab Emirates
[8]Faculty of Engineering Technology, Pagoh Higher Education Hub, Universiti Tun Hussein Onn Malaysia, Pagoh, Johor 84600, Malaysia

Corresponding authors: Abdulkadir Bello Shallah (shallah@graduate.utm.my), Farid Zubir (faridzubir@utm.my), and Noorlindawaty Md. Jizat (noorlindawaty.jizat@mmu.edu.my)

This work was supported in part by the Higher Institution Centre of Excellence (HICOE), Ministry of Higher Education Malaysia through the Wireless Communication Centre (WCC), Universiti Teknologi Malaysia (UTM), under Grant A.J091300.6800.09465 and Grant R.J090301.7823.4J610; and in part by the Faculty of Engineering, Multimedia University (MMU), Cyberjaya, Selangor, Malaysia.

ABSTRACT This paper introduces an innovative 4 × 4 dual-band Butler matrix (BM) characterized by compactness and an enhanced frequency ratio (K). The design employs meandered lines and an interdigital capacitor (IDC) unit-cell-based composite right/left-handed transmission-line (CRLH-TL) metamaterial (MTM) structure. The BM integrates compact dual-band 3 dB branch-line couplers (BLC), a 0 dB crossover, and dual-band ±45° phase shifters on a single Rogers RT5880 substrate having relative permittivity ε_r of 2.2 and thickness h of 0.787 mm. Simulations and measurement results demonstrate reflection and isolation coefficients exceeding −20 dB at all ports, with obtained insertion loss of −6±3 dB over the 0.7 GHz and 3.5 GHz frequency bands. The achieved output phase differences of ±45°, ±135°, ±135°, and ±45° at the designed frequencies indicate a maximum average phase tolerance of ±4.5° concerning the ideal values. Importantly, the BM's overall dimensions are 143 mm × 186 mm, resulting in an impressive 78% size reduction compared to traditional T-shaped BM designs. The proposed configuration is designed and simulated using CST Microwave Studio, with the agreement between simulated and measured parameters highlighting design reliability and effectiveness. Additionally, a performance evaluation comparing the proposed BM with existing circuits reveals its suitability for sub-6 GHz 5G dual-band antenna array beamforming networks (BFN) due to its compact size and improved band ratio.

INDEX TERMS Branch-line coupler, butler matrix, composite right/left-handed, crossover, frequency ratio, metamaterials, sub-6 GHz, 5G.

I. INTRODUCTION

As advancements in wireless communication technologies progress rapidly, there is a growing need for enhanced capacity and spectrum efficiency. The switched beam antenna array (SAA) has drawn significant attention over the past decades for its capability to mitigate multipath fading and suppress co-channel interference [1]. Various beamforming networks (BFNs), including the Rotman lens [2], Nolen matrix [3], Blass Matrix [4], and Butler Matrix (BM) [5],

The associate editor coordinating the review of this manuscript and approving it for publication was Guido Lombardi.

have been widely acknowledged. However, the Rotman lens is primarily employed in radar systems due to its substantial circuit size. Conversely, the Nolen matrix and Blass matrix, although efficient, require a larger number of fundamental elements that result in a complex, bulky structure and increased losses. Consequently, the BM emerges as a prominent choice for implementing a BFN due to its low loss and straightforward design. The typical BM, characterized by a symmetrical design, incorporates 3 dB branch-line coupler (BLC), 0 dB crossovers, and 45° phase shifter, having four input and output ports. When a specific input port is activated, it generates at the output ports signal with equal amplitude and a progressive-phase distribution, ensuring consistent phase differences (PD) (i.e., ±45° and ±135°) [6]. This capability enables the generation of four independent beams in the radiation pattern when a 4 × 4 BM is connected to an antenna array. Usually, when aiming to produce additional radiation beams with a single-band switched beam antenna array (SAA), a common approach is to increase the order of the BM network. This can be achieved by employing a higher-order BM, such as 8 × 8, 16 × 16, or beyond. Several studies have explored the design of high-order BMs [7], [8], [9].

However, increasing the order of the BM leads to an increased number of components and intersections of transmission lines (TLs). As a consequence, this undesirably increases the overall system's cost, size, complexity, and losses. Therefore, there is a need to explore innovative design concepts to address these challenges. A well-designed dual-band SAA system can achieve radiation beams at two specified frequencies without overlapping. By integrating a 4 × 4 dual-band BM feeding network with a four-elements dual-band linear array antenna, this configuration can provide an equivalent number of radiation beams as a single-band antenna array system with eight radiating elements. Typically, a dual-band SAA system with N elements can produce $2N$ radiation beams, leading to a substantial increase in capacity and size reduction [10].

A key role in the advancement of dual-band multiple beam arrays [10] and beam-switching systems [11] is played by a dual-band BM feeding network. The predominant approach for developing a dual-band BM involves converting each element of a single-band BM into a dual-band configuration. For instance, an initial dual-band BM design featured a dual-band BLC accompanied by two parallel coupled lines was reported in [12]. Another design in [11] utilized a dual-band 3 dB BLC having two sections, and a TL served the dual purpose of a 45° phase shifter. In [13], a Π-shaped TL was employed to develop a dual-band 3 dB BLC and a dual-band 45° phase shifter for the dual-band BM design. The use of a center frequency approach in [15] led to the development of a dual-band BLC, and a T-shaped TL was employed as a dual-band phase shifter for the design of a dual-band BM. In [14], [16], and [17], a 4 × 4 dual-band BM was introduced, with designs that eliminated the need for crossings. Furthermore, in [18], a dual-band filtering BM was developed to operate at 12 GHz and 17 GHz by integrating a resonator with stub-loading.

The studies above illustrates the operation of dual-band functions, predominantly achieved size reduction by removing crossovers. However, the removal of crossings results in increased circuit complexity for large BM networks (8×8, 16×16), adversely affecting output parameters at lower frequencies, as indicated in [19]. Additionally, the dual-band frequency ratio (K) is relatively small. On the other hand, in [20] and [21], the analysis of BM using metamaterial (MTM) TL was conducted at various frequencies, examining size reduction, bandwidth enhancement, dual-band operation, and the variation of performance parameters to frequency changes. The application of MTM-TL to the BM network is relatively simple, and its performance remains unaffected even when the order is increased to 8 × 8 or beyond. This is because the MTM-TL properties were introduced without modifying the traditional BM layout [22].

This paper presents a new 4 × 4 dual-band BM using the MTM-TL technique. The design incorporates four dual-band BLCs employing the meandered-line technique and an interdigital capacitor (IDC) MTM-TL structure. Unlike traditional BMs with two 0 dB crossovers, our design features a single 0 dB dual-band crossover, along with two dual-band ±45° phase shifters. The contributions of our proposed design can be summarized as follows: 1) It is the first fully dual-band BM incorporating the MTM-TL structure reported in the literature; 2) It achieves the widest frequency band ratio to date; 3) It exhibits low complexity due to a reduced number of components compared to conventional designs. The designed BM demonstrates excellent performance in both simulation and measurement results and can generate eight non-overlapping beams, making it an ideal candidate for the dual-band BFN in 5G antenna array systems.

II. BUTLER MATRIX DESIGN ANALYSIS

Fig. 1, illustrates the proposed 4 × 4 dual-band Butler matrix (BM), comprising of four 3 dB dual-band branch-line couplers (BLCs), two ±45° dual-band phase shifters, and one 0 dB dual-band crossover. The BM features four input ports (Port 1−Port 4) and four output ports (Port 5−Port 8). When any input port is excited, the signal divides into four output signals with equal amplitude. However, there is a progressive phase difference (PD) of ±45° and ±135° between the output ports, determined by the operating frequency and excitation port. The symmetry of the proposed BM ensures that the PD between the output ports remains the same, whether the excitation is between Port 3 and Port 4 or between Port 1 and Port 2. However, the signs of the PD are opposite in these respective cases, and the output PDs at each frequency band are listed in Table 1.

A. DUAL-BAND BRANCH-LINE COUPLER

In section I, the common method for realizing a dual-band BM was discussed, which involves converting individual

TABLE 1. Output phase response and progressive phase differences.

	Lower frequency (f_1)					Upper frequency (f_2)				
Port Number	P_5	P_6	P_7	P_8	**PD**	P_5	P_6	P_7	P_8	**PD**
Port 1	135°	90°	45°	0°	**−45°**	−135°	−90°	−45°	0°	**+45°**
Port 2	45°	180°	−45°	90°	**+135°**	−45°	−180°	45°	−90°	**−135°**
Port 3	90°	−45°	180°	45°	**−135°**	−90°	45°	−180°	−45°	**+135°**
Port 4	0°	45°	90°	135°	**+45°**	0°	−45°	−90°	−135°	**−45°**

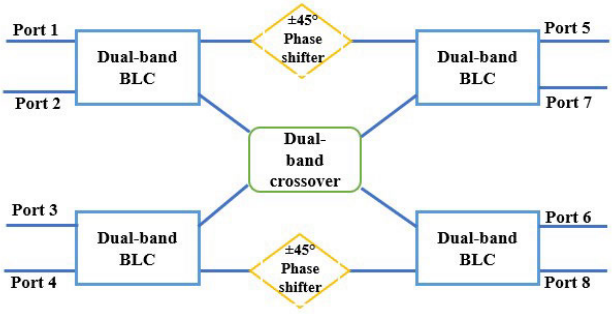

FIGURE 1. The circuit layout of the proposed 4 × 4 dual-band BM.

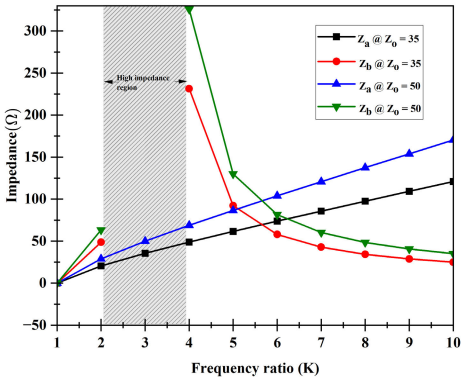

(a)

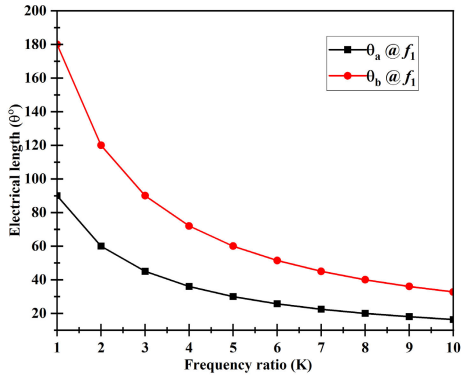

(b)

FIGURE 2. Relationships between (a) Line impedances and frequency ratio (K) (b) Electrical length and frequency ratio (K).

elements of a single-band BM into a dual-band configuration. This conversion process involved the addition of extra stubs, specifically in the form of Π or T sections. The standard λ/4 TL characterized by (Z_o, θ_o) is replaced with T-shaped sections, each comprising two horizontal TLs of (Z_a, θ_a) and an open stub of (Z_b, θ_b) determined at frequency f_1. This structure is obtained by equating the ABCD matrix of the standard λ/4 TL to the ABCD matrix of the T-shaped sections, as in the Equations (1)−(3) [23].

$$A_T = D_T = \cos^2\theta_a - \sin^2\theta_b - \frac{Z_a \sin\theta_a \cos\theta_a \tan\theta_b}{Z_b} \quad (1)$$

$$B_T = 2jZ_a \cos\theta_a \sin\theta_a - j\frac{Z_a^2 \sin^2_{\theta a} \tan\theta_b}{Z_b} \quad (2)$$

$$C_T = \frac{2j \sin\theta_a \cos\theta_b}{Z_a} + \frac{j\cos^2\theta_a \tan\theta_b}{Z_b} \quad (3)$$

The BLC discussed in this research builds upon the design in [24], so a comprehensive solution of the Equations (1)−(3) can be referred to for the reader's understanding. The variations in characteristic impedances, with K, as well as electrical lengths, with the K, are illustrated in Figs. 2(a) and 2(b), respectively. The practical impedance range for (Z_a, Z_b), spans from (22.5 Ω−180 Ω), with the corresponding K limited within the ranges of (1.93−2.33) and (3.5−8.7). However, achieving ratios between 2.34 and 3.49 presents a challenge due to the high impedance experienced in this range.

Fig. 3 depicts the initial design stage of the dual-band BLC (conventional T-shaped), which operates at both 0.7 GHz and 3.5 GHz, and occupy a considerable amount of space based on the calculated design parameters. The stubs are excessively long, posing challenges for seamless integration into the design. Consequently, several right-angle bends have been introduced, and these bends are further chamfered to reduce the capacitive effects associated with the angles [25]. The T-section dual-band BLC is then reduced to a total circuit area of (74.2 mm × 66.2 mm), as illustrated in Fig. 4

Likewise, adjustments were made to the BLC's series and shunt TL segments to achieve additional size reduction using the meandering technique outlined in [26]. This technique involved integrating four right-angle bends into each arm, where each bend covered an approximate path length of πR/2 mm as shown in Fig. 5. Consequently, the combined path length of all four bends in each arm equated to

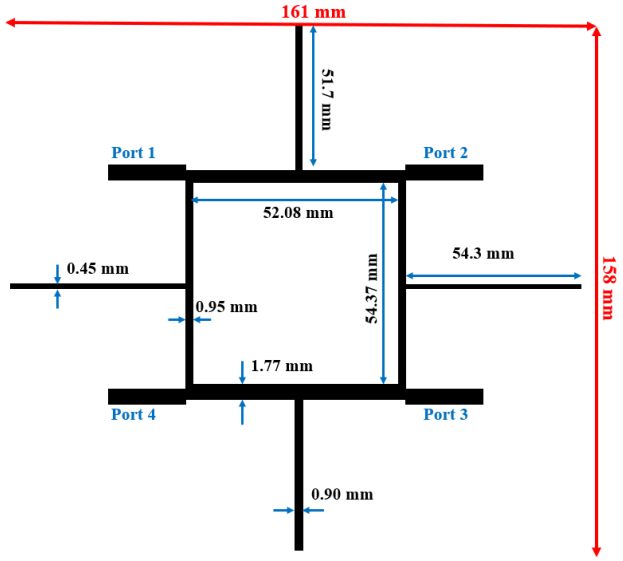

FIGURE 3. The dual-band BLC termed as conventional stub tabbed.

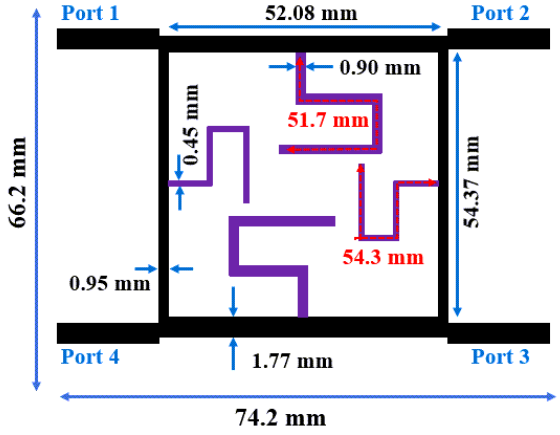

FIGURE 4. The dual-band BLC with folded stubs.

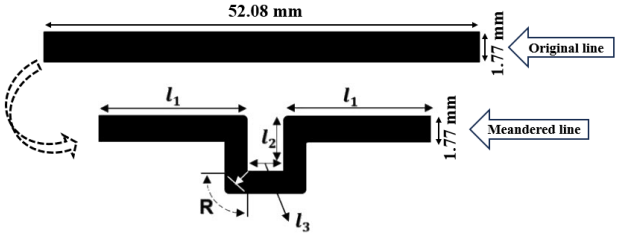

FIGURE 5. The schematic illustration depicts the process of meandering the series arm of the BLC.

2πR mm. Here, R represents the mean radius of the line, whereas the width of line remained unchanged. The MTM dual-band BLC was developed using meandered lines, stubs, and IDC unit cells for both the vertical and horizontal arms of the BLC. For the IDC unit-cell design, the detailed theoretical analysis and the optimized dimensions, including total capacitance C, finger width (f_w), length (f_l), and gap (s), using the Equations (4)-(6) [27], [28].

$$C = (\varepsilon_r + 1) \times fl \times [(N_f - 3)A_1 + A_2]\,(pF) \tag{4}$$

$$A_1 = 4.409 \tanh\left[0.55\left(\frac{h}{Bw}\right)^{0.45}\right] \times 10^{-6}(pF/\mu m) \tag{5}$$

$$A_2 = 9.92 \tanh\left[0.52\left(\frac{h}{Bw}\right)^{0.5}\right] \times 10^{-6}(pF/\mu m) \tag{6}$$

where N_f is the number of fingers, ε_r represents the relative permittivity of the substrate, and constants A_1 and A_2 correspond to the interior and exterior sections of the IDC fingers with respect to the substrate height h and base width of the IDC fingers Bw.

Therefore, once the desired number of fingers is decided, the parameters f_w, f_l, and $s = 2f_w/3$ can be determined using the Equations (7) and (8).

$$f_w \approx \frac{Bw}{\left(\frac{5N_f}{3} - \frac{2}{3}\right)} \tag{7}$$

$$fl \approx \frac{\lambda_g}{8} \approx \frac{c}{8f_o\sqrt{\varepsilon_r}} \tag{8}$$

The properties of IDC's MTM unit-cell are determined through the Nicolson Ross Weir (NRW) method [29], a technique employed to derive the ε and μ values from the S-parameters. The term "left-handed MTMs (LH-MTMs)" refers to materials exhibiting negative ε and μ concurrently within specific frequency ranges. The NRW method acquires the ε and μ by utilizing the following constants:

$$V_1 = S_{21} + S_{11} \tag{9}$$

$$V_1 = S_{21} - S_{11} \tag{10}$$

$$X = \frac{1 - V_1V_2}{V_1 - V_2} \tag{11}$$

It can be demonstrated that Γ can be derived from the scattering coefficients by selecting the appropriate sign, ensuring that Γ is less than 1, as follows:

$$\Gamma = X \pm \sqrt{X^2 - 1} \tag{12}$$

$$z = \frac{V_1 - \Gamma}{1 - V_1\Gamma} \tag{13}$$

$$c_1 = \left(\frac{1 + \Gamma}{1 - \Gamma}\right)^2 = \frac{\mu_r}{\varepsilon_r} \tag{14}$$

$$c_2 = -\left[\frac{c}{wd} ln\left(\frac{1}{z}\right)\right]^2 = \mu_r\varepsilon_r \tag{15}$$

Subsequently,

$$\mu_r = \sqrt{c_1c_2} \tag{16}$$

$$\varepsilon_r = \sqrt{\frac{c_2}{c_1}} \tag{17}$$

Fig. 6 displays the extracted ε and μ parameters of the IDC unit-cell for the proposed MTM-based BLC. It illustrates that both ε and μ exhibit negative values simultaneously across the frequency range of 0.2 GHz to 2.6 GHz, aligning

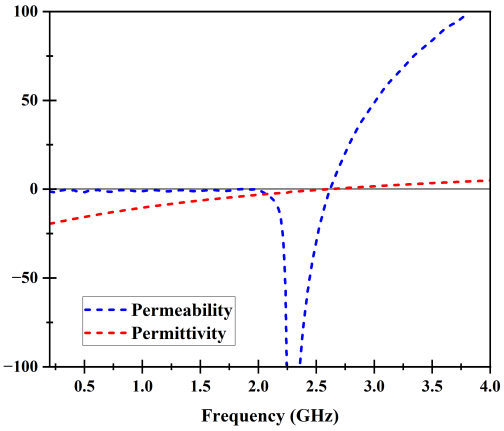

FIGURE 6. Extracted ε and μ parameters of proposed MTM based BLC unit-cell.

TABLE 2. The optimized dimensions of the proposed BLC and IDC unit-cell.

Section	Description	Parameter	Dimension (mm)
Series line	Width of BLC	W	50
	First division	w_1	11.4
	Second division	w_2	4.36
	Third division	w_3	9.12
Shunt line	Width of BLC	L	48
	First division	l_1	10.7
	Second division	l_2	5.7
	Third division	l_3	9.0
IDC	Base width	Bw	5.7
	Base length	Bl	0.3
	Finger length	fl	2.7
	Finger width	fw	0.3
	Inter-finger space	s	0.3
	Finger end gap	g	0.3

with the operational frequency of the device. The unit cell was designed to provide a miniaturization effect at lower frequencies, as electromagnetic structures designed for low frequencies are typically large. This demonstrates that the unit cell exhibits MTM-TL characteristics within the lower frequency band.

The proposed BLC operates at dual-band frequencies of 0.7 GHz and 3.5 GHz. To achieve the desired performance and simultaneously reduce the overall size of the structure, the dimensions of the lines, stubs, and IDC were optimized and provided in Table 2. Fig. 7(a-b) illustrates the diagram and photograph of the proposed BLC, showing port numbers and dimensions, which is 90% less than the conventional T-shaped dual-band BLC operating in the same frequency bands. This optimization ensures that the BLC meets the required performance criteria while maintaining a significantly reduced size compared to traditional T-shaped dual-band BLCs.

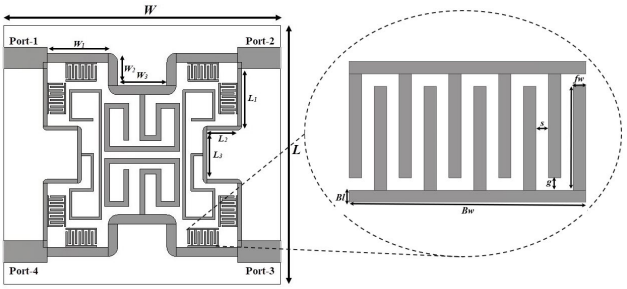

(a)

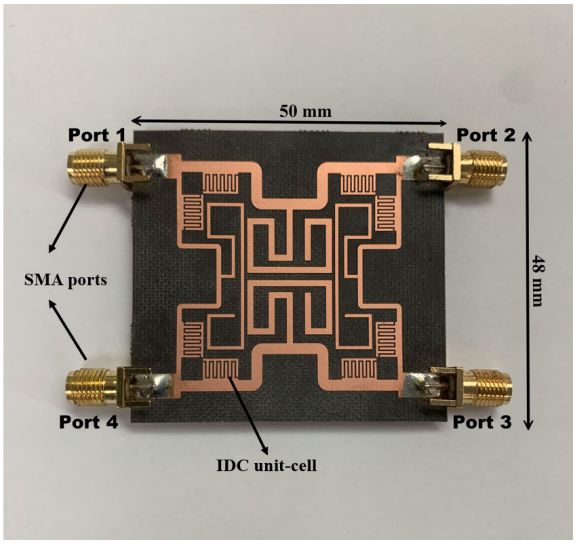

(b)

FIGURE 7. The proposed dual-band BLC (a) displaying the zoom-in IDC unit-cell (b) The fabricated prototype on rogers RT5880 substrate.

The BLC holds substantial importance in the design of the BM. Figs. 8(a-c) presents the performance of the proposed dual-band MTM based BLC in terms of S-parameter characteristics and phase response among the output ports. In Fig. 8(a), simulation and measurement results demonstrates the effective operation of the proposed BLC at the frequency bands of 0.7 GHz and 3.5 GHz. The simulated and measured characteristics of return-loss S_{11} and isolation-loss S_{41} at both frequencies in the proposed design are better than −20 dB. Simultaneously, for achieving equal power division between Port 2 and Port 3, the BLC design necessitates insertion loss S_{21} and coupling loss S_{31} to be around − 3dB. The simulated and measured results for S_{21} and S_{31}, depicted in Fig. 8(b), show approximately −2.76 dB/−3.06 dB, −3.4 dB/−3.52 dB, at lower frequency, and −3.05 dB/−3.09 dB −3.9 dB/−2.88 dB at upper frequency bands, respectively. The average insertion loss error is 0.26 dB, and for coupling loss, it is 0.4 dB, aligning closely with the desired value of −3 dB. Therefore, the proposed BLC attained a coupling factor of approximately −3±0.5 dB for each frequency band. In Fig. 8(c), it is shown that the simulated and measured PDs between Port 2 and Port 3 are −89.9°/−89.0° and 88.5°/90.1° at 0.7 GHz and 3.5 GHz, respectively. As a result, the average phase

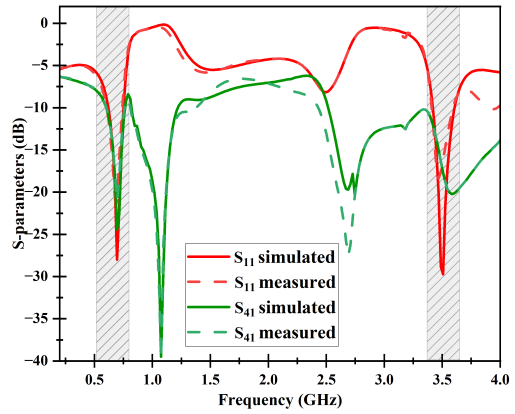

(a)

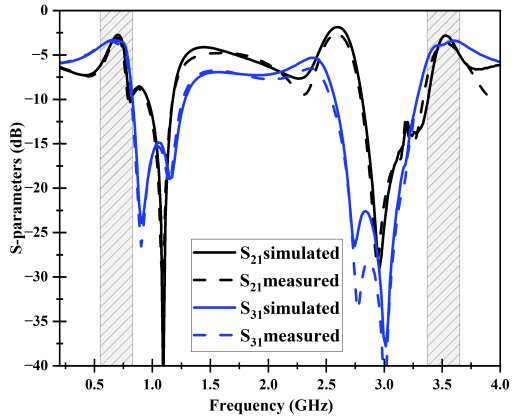

(b)

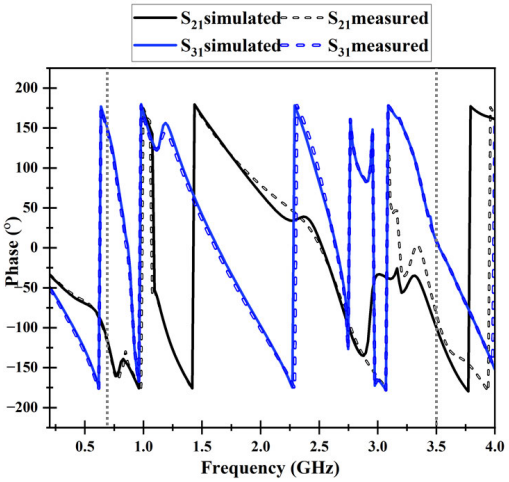

(c)

FIGURE 8. The S-parameters characteristics of the proposed BLC (a) S_{11} and S_{41} (b) S_{21} and S_{31} (c) phase response.

error (PE) is 1.3°, indicating a slight variation from the desired value of 90°.

B. DUAL-BAND ±45° PHASE SHIFTER

The dual-band transmission lines (TLs) were employed to function as the 45° dual-band phase shifter with a

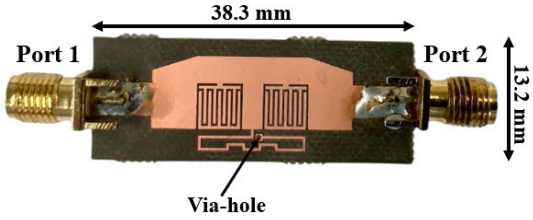

FIGURE 9. The photograph of the fabricated proposed ±45° dual-band phase shifter.

T-shaped configuration. In this structure, Z_a and Z_b represents the characteristic impedances of the horizontal and vertical lines, respectively. Additionally, θ_a and θ_b denotes the corresponding electrical lengths at the frequency f_1. Utilizing the ABCD-matrix of the T-shaped structure and Equations (1)−(3), it is determined that θ_a and θ_b can be substituted with $(n\pi - \theta_a)$ and $(2m\pi - \theta_b)$, where n and m are integers to maintain A_T while making B_T opposite, (A_T and B_T are parameters in the ABCD-matrix of the T-shaped structure). This serves as a crucial aspect for achieving dual-band operation. In our specific design, the electrical lengths of the line and stub are denoted as "θ_a and θ_b" and "$n\pi - \theta_a$ and $2m\pi - \theta_b$" at f_1 and f_2 frequencies, respectively [30].

After a series of derivations, the ultimate formulas for θ_a and θ_b are presented as in Equation (18). Through the application of $A_T = A_P$ and $B_T = B_P$ (where A_P and B_P are parameters in the ABCD-matrix of the ideal 45° phase-shifting line), the values of Z_a and Z_b can be derived. In the proposed design, the parameter values are as follows: $\theta_a = \theta_b = 60°$, $Z_a = 89.97\ \Omega$, and $Z_b = 46.81\ \Omega$.

$$\theta_a = \frac{f_1}{f_1 + f_2} \times n\pi\ @f_1,\ \theta_b = \frac{f_1}{f_1 + f_2} \times 2m\pi\ @f_2 \qquad (18)$$

whereas the dual-band 45° phase shifter designed with the specified parameters effectively operates at the desired frequencies, its overall size is notably large, measuring 107.2 mm × 72.1 mm. A composite right/left handed (CRLH) TL utilizing the interdigital capacitor (IDC) unit cell [31] was integrated into the design to enhance its performance and minimize its footprint. Additionally, the long open stub is replaced with a meandered stub shortened using via, and the miniaturized dimensions were obtained as 38.3 mm × 13.2 mm, which is about 93% less than the conventional T-shaped design. The fabricated prototype is shown in Fig. 9, while the specific parameter values for the IDC and the miniaturized structure are listed in Table 3.

Fig. 10(a), shows the S-parameter magnitude responses of the proposed dual-band phase shifter. In terms of both the simulated and measured results, S_{11} is below −15 dB and S_{21} is close to 0 dB, achieving the values of −0.13 dB/−0.05 dB and −0.23 dB/−0.6 dB across 0.7 GHz and 3.5 GHz frequency bands, respectively. Whereas in Fig. 10(b), the simulated and measured phase shifts at the lower band 0.7 GHz are −44.6°/−43.3°, and +45.8°/+43.6° were

TABLE 3. Dimensions of the miniaturized 45° dual-band phase shifter.

±45° phase shifter						
Parameter.	L (mm)	W (mm)	l_1 (mm)	l_2 (mm)	l_3 (mm)	w_1 (mm)
Values	38.2	13.2	5	2.7	1.95	1.8
IDC unit cell						
Parameter.	Bw (mm)	fl (mm)	fw (mm)	s (mm)	g (mm)	-
Values	4.83	4	0.3	0.3	0.3	-

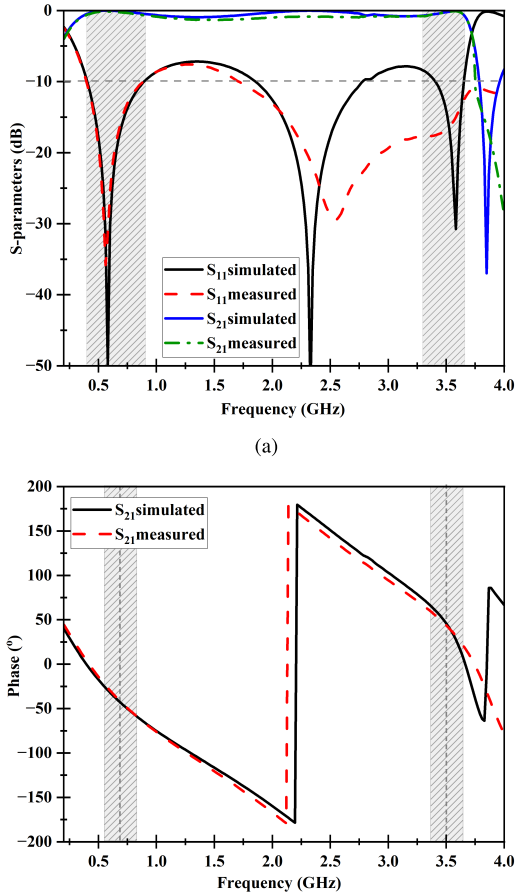

FIGURE 10. Proposed ±45° phase shifter (a) S-parameters magnitude response (b) Phase response.

achieved at the upper-frequency band 3.5 GHz. This indicates that the maximum measured phase deviation is not more than 1.7°.

C. DUAL-BAND CROSSOVER

The traditional 0 dB crossover functions as a four-port network, comprising Port 1, Port 2, Port 3, and Port 4. When an input signal is applied to Port 1, the signal is directed to Port 3, and activation of Port 2 routes the signal to Port 4. In an ideal scenario, the perfect crossover would display no insertion loss at the diagonal ports S_{31}/S_{24} and maintain high isolation between neighboring ports S_{41}/S_{23}. However, achieving zero

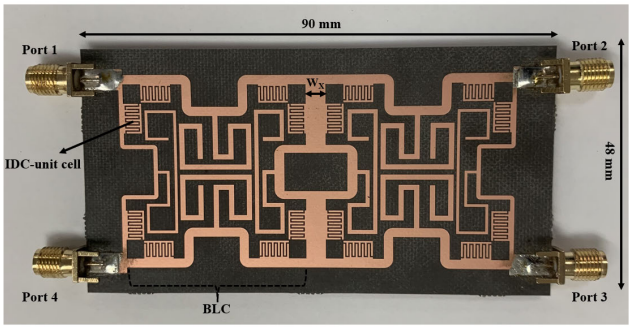

FIGURE 11. The photograph of the fabricated proposed 0 dB dual-band crossover.

insertion loss in practical applications poses a challenge and requires an exact design approach to minimize it.

The proposed crossover was achieved by combining two BLCs from section II-A in cascade, and Fig. 11 shows the fabricated prototype of the crossover configuration. It is important to highlight that the dimensions of the IDC and the stub lines in the crossover were kept consistent with those used in the BLCs. The middle section width (W_x = 3.8 mm) of the crossover was optimized to obtain resonance within the specified frequency ranges. The overall dimensions of the crossover are 90 mm × 48 mm.

Figs. 12(a) and 12(b) illustrates the performance of the proposed 0 dB dual-band crossover, specifically focusing on S-parameters and phase differences between the adjacent output ports. At both the 0.7 GHz and 3.5 GHz frequency bands, the simulated and measured return-loss S_{11} characteristics achieved were below −16 dB as shown in Fig. 12(a). In terms of insertion-loss at diagonal ports, the values obtained for both S_{31} and S_{24} at 0.7 GHz were −0.29 dB. Similarly, at an operating frequency of 3.5 GHz, the values were −0.23 dB for S_{31} and S_{24}. Likewise, the phase differences between S_{31} and S_{24} as obtained through simulation and measurement, illustrated in Fig. 12(b), remains consistently close to the ideal value of 0°.

D. 4×4 DUAL-BAND BUTLER MATRIX

A dual-band capable miniaturized 4 × 4 Butler Matrix (BM) was realized by integrating four previously developed dual-band branch-line couplers (BLCs). This design utilizes meandered lines and an interdigital capacitor-composite right/left-handed transmission line (IDC-CRLH TL). The structure features a 0 dB dual-band crossover and two ±45° dual-band phase shifters, operating at frequencies of 0.7 GHz and 3.5 GHz. With a total of eight ports, the device includes four input ports (Port 1, Port 2, Port 3, and Port 4), while the remaining four ports (Port 5, Port 6, Port 7, and Port 8) serve as output ports, making the BM a 4 × 4 network.

Figure 13(a) illustrates the prototype of the proposed 4 × 4 dual-band BM, which has been implemented on a single Rogers RT5880 substrate with a dielectric constant of 2.2, a loss tangent of 0.0009, and a thickness of 0.787 mm. The selection of the substrate is motivated by

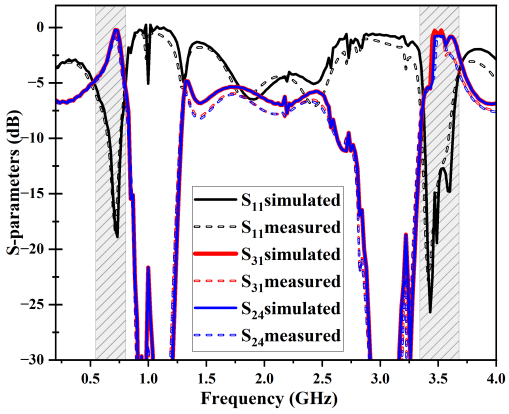

(a)

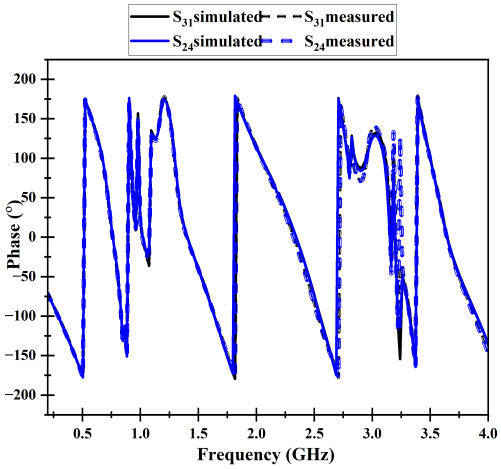

(b)

FIGURE 12. (a) S-parameter response of the simulated and measured crossover (b) phase response of the simulated and fabricated crossover.

the significant reduction in bandwidth observed at the lower band of 0.7 GHz, and RT5880 is chosen for its low-loss properties and enhanced bandwidth capabilities [32]. The overall dimensions of the structure are 143 mm × 186 mm. When a signal is applied to any input port of the BM, it evenly divides among the four output ports, with transmission coefficients approximately within the range of −6 dB, and a return loss exceeding −10 dB across the entire bandwidth. To obtain the measured S-parameter results of the developed BM, a Rohde & Schwarz (ZVB-20) Vector Network Analyzer (VNA) was employed. This analyzer is capable of operating across frequencies ranging from 10 MHz to 20 GHz. In Fig 13(b), a photograph of the Device Under Test (DUT) utilizing the VNA is presented. Throughout the measurements, all unused ports were terminated with a 50 Ω SMA terminator.

III. RESULT DISCUSSION

Figs. 14, and 15 displays both the simulated and measured S-parameter results of the 4 × 4 Butler Matrix (BM) for Port 1 and Port 2 excitation. In Fig. 14(a) and 14(b) the

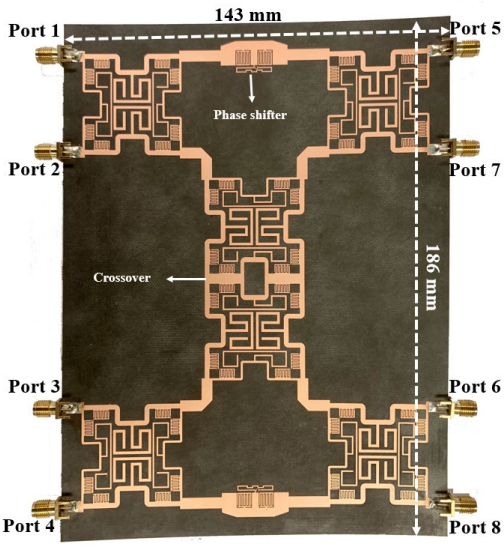

(a)

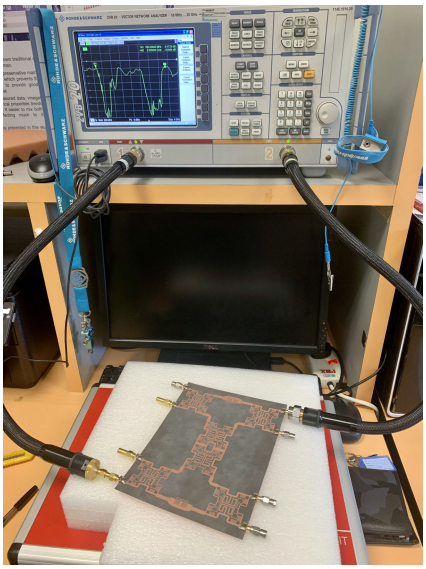

(b)

FIGURE 13. The fabricated prototype of (a) the proposed 4 × 4 dual-band BM (b) BM as a device under test.

reflection coefficients of more than −19 dB and −16 dB have been achieved for 0.7 GHz and 3.5 GHz, with the isolation coefficients for Port 1 excitation presented in Fig. 14(c). The transmission coefficients for Port 1 excitation are depicted in Figs. 15(a) and 15(b), whereas those for Port 2 excitation are illustrated in Figs. 15(c) and 15(d) for the proposed BM output ports. In both cases, the transmission coefficients closely match the theoretical −6 dB value. A minor variation within the range of ±3 dB is observed when the signal is applied to both Port 1 and Port 2 across the two frequency bands, as detailed in Table 4. The symmetry of the proposed structure ensures that the transmission coefficients remain unchanged when Port 3 and Port 4 are excited. Consequently, there is no need to present the results of transmission

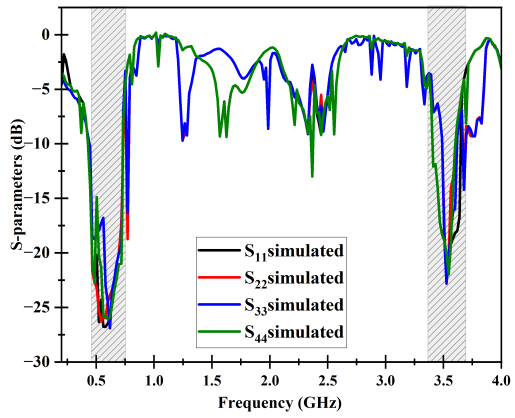

(a)

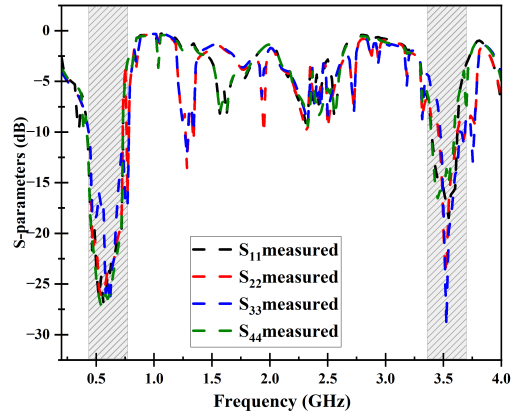

(b)

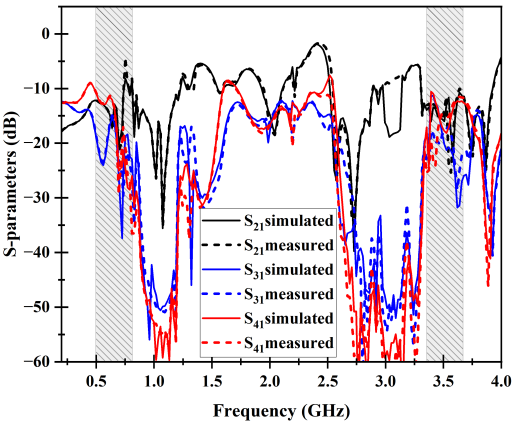

(c)

FIGURE 14. Reflection coefficients and (a) simulated (b) measured (c) Isolation coefficients of the proposed BM.

coefficients at the output ports for the excitation of Port 3 and Port 4.

To ensure that the dual-band 4 × 4 BM adheres to the specified progressive phase differences as per theoretical values, the phase difference (PD) between adjacent ports at the output of the proposed BM are illustrated in Figs. 16 and 17. Fig. 16(a) and 16(b) compare the simulated and measured results for the dual-band BM when Port 1 is excited at f_1 and f_2, respectively. Whereas Fig. 17 presents the phase difference for Port 2 excitation. As indicated in Table 5, when Port 1 is activated, the progressive phase difference at output Ports 5, 6, 7, and 8 is $-45°$ at 0.7 GHz and $+45°$ at 3.5 GHz. On the other hand, activating Port 2 results in phase differences of $+135°$ and $-135°$ at 0.7 GHz and 3.5 GHz with phase tolerance of $\pm 4.5°$, respectively. Complementary phase responses for input Ports 3 and 4 can be generated at both frequencies.

IV. COMPARISON STUDY

Table 6 presents a comprehensive comparative analysis, evaluating various existing structures of Butler Matrix (BM) designed for dual-band applications within sub-6 GHz frequency bands. Additionally, a few recent MTM-based single-band structures [36], [37] with a size reduction of 74%, and 76% are included in the assessment. The results underline the effectiveness of the proposed design, revealing significantly lower complexity compared to most existing BM designs. The proposed BM design is a single-layer structure, maintaining a conventional BM layout while adeptly executing dual-band operations up to the 5-band ratio. The findings highlight not only its operational efficiency but also its capacity to simplify the implementation of dual-band functionalities.

Moreover, when extended to higher-order matrices, the proposed design can demonstrates a remarkable reduction in complexity compared to the approaches outlined in Table 6. This reduction is particularly notable, given that many reported designs achieve size reduction by eliminating crossovers. Although this size reduction approach has been adopted by others, it often complicates the circuit and presents challenges when integrating antennas on the same layer [20], [33]. In contrast, the proposed BM strikes a balance by reducing size and complexity without compromising performance.

It is crucial to emphasize the wider band ratio achieved by the proposed BM, making it as a standout choice for sub-6 GHz 5G dual-band applications. In comparison to the conventional T-shaped design, the proposed BM demonstrates an impressive 78% reduction in size. This reduction contributes not only to a more compact overall system but also signifies a substantial advancement in resource utilization and spatial efficiency. Consequently, the proposed design emerges as a promising solution, offering a compelling combination of simplicity, efficiency, and size reduction for 5G dual-band switched-beam array antenna applications.

V. POTENTIAL INTEGRATION WITH A 1 × 4 LINEAR ANTENNA ARRAY

Fig. 18 illustrates the potential connection of the proposed BM to a 1 × 4 linear antenna array. It is important to highlight that this paper does not incorporate an antenna array;

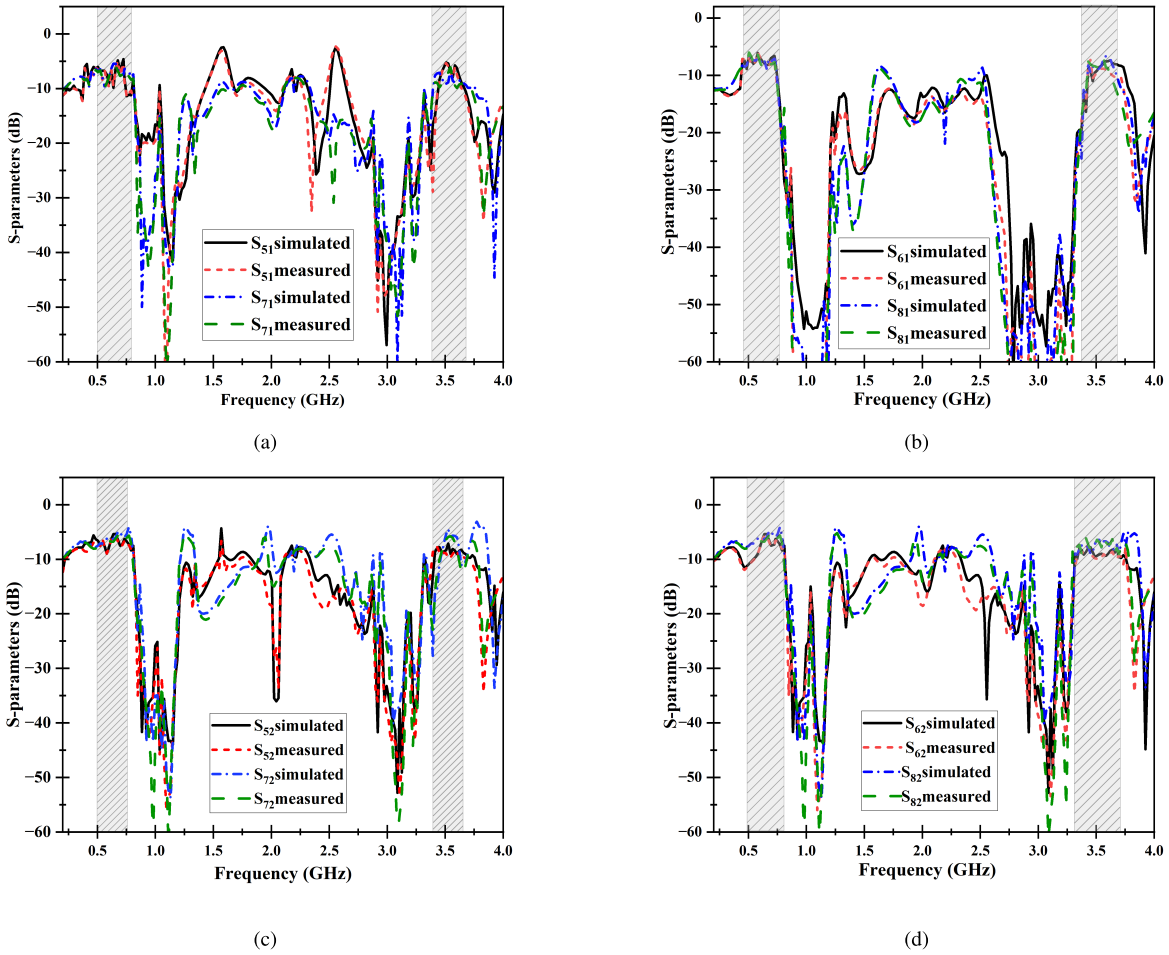

FIGURE 15. The transmission coefficients of the proposed BM at f_1 and f_2 for (a-b) Port 1 excitation (c-d) Port 2 excitation.

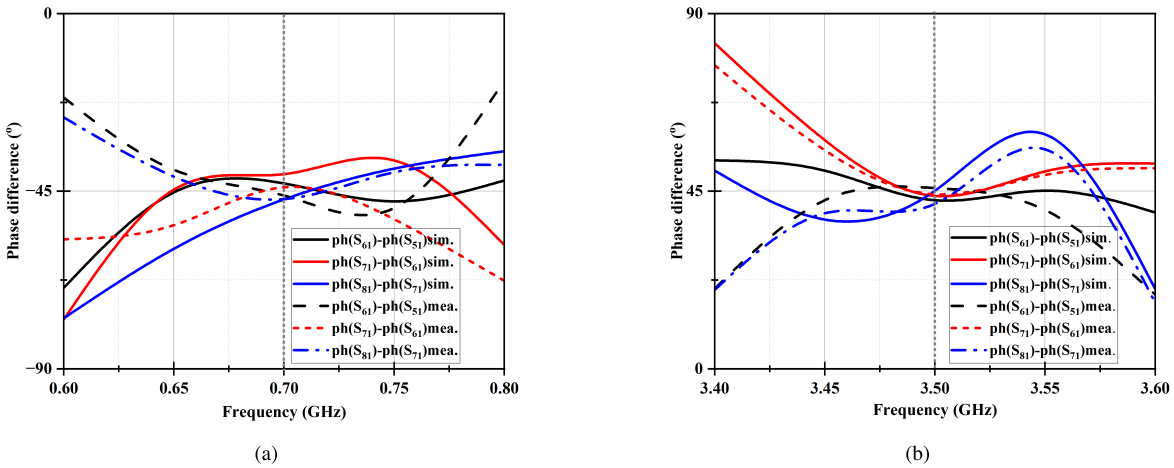

FIGURE 16. The diagram of the phase difference between the adjacent output ports for Port 1 excitation (a) lower band (b) upper band.

however, the calculated radiation beam angle is provided for the reader's understanding. To achieve a compact size, the entire switched-beam array antenna (SAA) system adopts to a dual-band operation approach. This requires that both the 4 × 4 BM and the antenna array are designed to operate in dual frequency bands. Likewise, the frequency ratio plays a crucial role in the overall system design. Assuming a BM structure with output signal PDs (Φ) of $\pm 45°$ and $\pm 135°$, the

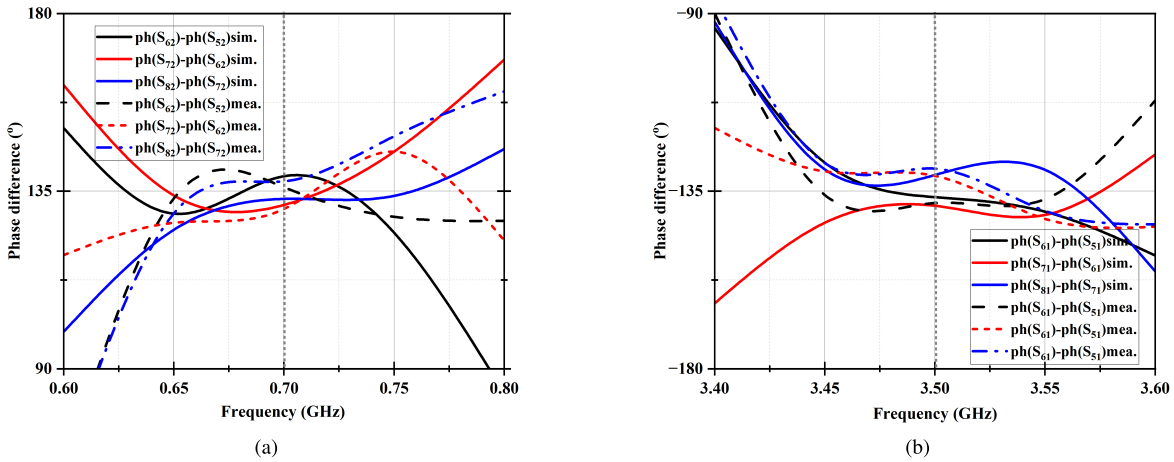

FIGURE 17. The diagram of the phase difference between the adjacent output ports for Port 2 excitation (a) lower band (b) upper band.

TABLE 4. Transmission coefficients of the proposed BM for Port 1 and Port 2 excitation at 0.7 GHz and 3.5 GHz.

Input Port	Transmission Coefficient (dB) @ f_1= 0.7 GHz				Transmission Coefficient (dB) @ f_2= 3.5 GHz				
Port 1	S_{51}	S_{61}	S_{71}	S_{81}	S_{51}	S_{61}	S_{71}	S_{81}	**Required value (dB)**
Simulated	−6.06	−6.87	−7.44	−7.43	−5.52	−8.30	−8.10	−8.90	−6 ± 3
Measured	−6.78	−7.48	−8.82	−6.66	−8.41	−6.81	−7.49	−8.23	−6 ± 3
Port 2	S_{52}	S_{62}	S_{72}	S_{82}	S_{52}	S_{62}	S_{72}	S_{82}	**Required value (dB)**
Simulated	−7.43	−6.28	−5.23	−6.82	−8.54	−8.57	−6.02	−5.90	−6 ± 3
Measured	−6.79	−6.62	−6.76	−6.67	−6.91	−7.85	−8.01	−8.11	−6 ± 3

TABLE 5. Output phase difference of the proposed BM for Port 1 and Port 2 excitation at 0.7 GHz and 3.5 GHz.

Input Port	Frequency f_1= 0.7 GHz			Frequency f_2= 3.5 GHz			
Port 1	**(5/6)**	**(6/7)**	**(7/8)**	**(5/6)**	**(6/7)**	**(7/8)**	**Ideal value**
Simulated	−39.8°	−47.2°	−41.1°	49.7°	42.6°	38.5°	±45°
Measured	−46.1°	−44.0°	−47.0°	48.8°	44.2°	41.8°	±45°
Port 2	**(5/6)**	**(6/7)**	**(7/8)**	**(5/6)**	**(6/7)**	**(7/8)**	**Ideal value**
Simulated	138.8°	131.2°	129.3°	−130.2°	−133.6°	−131.4°	±135°
Measured	136.0°	128.9°	137.5°	−138.0°	−131.1°	−129.3°	±135°

main beam angle θ can be determined by applying the array factor [34], as follows:

$$\Phi = \pm 45^\circ,\ \cos\theta = \left(n \pm \frac{1}{8}\right) N \tag{19}$$

$$\Phi = \pm 135^\circ,\ \cos\theta = \left(n \pm \frac{3}{8}\right) N \tag{20}$$

Having n as an integer (0, ±1, ±2, …), N is defined as λ/d, where d represents the spacing between elements, and λ is the wavelength at the designed frequency. It is important to note that in the proposed design, which involves two operating frequencies, there will be two distinct values of N corresponding to these frequencies.

The calculated radiation beam angles of the array antenna based on the PD between the adjacent ports of the BM at operating frequencies of 0.7 GHz and 3.5 GHz are presented in Table 7. These values were determined using the process outlined in [34] and [35]. As illustrated in Fig. 18, different radiation beam angles θ can be produced by different values of N.

TABLE 6. A comparative analysis with the state-of-the-art related works designed to operate at dual-band frequencies.

Ref./Year	f_1/f_2(GHz)	Band ratio	Size reduction (%)	Method
[10]/2016	2.4/5.2	2.17	–	Multi layer
[14]/2016	1.85/2.7	1.46	–	No crossover
[16]/2019	1/2.5	2.5	–	No crossover
[17]/2020	1/2.85	2.85	–	No crossover
[36]/2022	3.5	N/A	76	MTM-TL
[37]/2024	3.5	N/A	74	MTM-TL
This work	**0.7/3.5**	**5**	**78**	**MTM-TL**

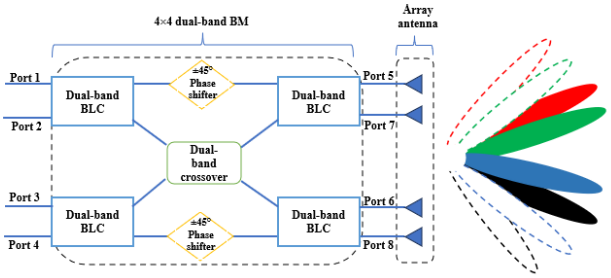

FIGURE 18. The circuit layout of the proposed 4 × 4 dual-band BM connected to 1 × 4 array antenna. (Note: The dash lines represent the beams generated at f_1, while solid lines are the beams produced at upper frequency f_2).

TABLE 7. Progressive phase differences and calculated beam angles.

	Lower frequency (f_1)		Upper frequency (f_2)	
Port Number	$\Delta\Phi^\circ$	θ°	$\Delta\Phi^\circ$	θ°
Port 1	−45	−19	+45	+4
Port 2	+135	+12.8	−135	−11.2
Port 3	−135	−12.8	+135	+11.2
Port 4	+45	+19	−45	−4

Since the proposed SAA system operates in dual-band frequency bands, there are two unique ratio parameters, N_1 and N_2, corresponding to the lower frequency f_1 and the upper frequency f_2, respectively. Therefore, according to Fig. 18, there should be four different radiation beam angles corresponding to each of the dual operating frequencies (f_1 and f_2) for each PD of $\Phi = \pm 45^\circ$ and $\Phi = \pm 135^\circ$ because d are the same at these two frequencies. To achieve the optimal frequency ratio (f_2/f_1), λ_1 and λ_2 are defined as the wavelengths at f_1 and f_2, respectively. Given that the $d = \lambda_1/N_1 = \lambda_2/N_2$, the frequency ratio can be expressed as $f_2/f_1 = N_1/N_2$. It is important to note that, to minimize the generation of undesirable grating lobes, the recommended range for N in this case lies between the ratio 0.52 and 2.6. Beyond this range, multiple main beam angles may be generated by the Equations (19) and (20). As a result, the proposed SAA has the capability to produce eight different radiation beams without any overlap. This functionality allows it to achieve performance levels similar to those of a traditional phased array antenna (PAA) system employing a single-band 8 × 8 BM network [38].

VI. CONCLUSION

In conclusion, this paper presents a novel 4 × 4 dual-band Butler matrix (BM) that achieved remarkable compactness and an enhanced frequency band ratio. The innovative design incorporates meandered lines and an interdigital capacitor (IDC) unit cell, creating a composite right/left handed transmission line (CRLH-TL) structure. The BM integrates dual-band 3 dB BLCs, a 0 dB crossover, and a dual-band ±45° phase shifter on a single Rogers RT5880 substrate. Simulations and measurements validated its exceptional performance, with reflection and isolation coefficients exceeding −20 dB at all ports and a promising insertion loss of −6±3 dB across the 0.7 GHz to 3.5 GHz bands.

The achieved phase differences exhibit a maximum average tolerance of ±4.5°, underscoring the precision of the design. Importantly, the BM's compact dimensions of 143 mm × 186 mm represent a remarkable 78% size reduction compared to traditional T-shaped BM designs. The paper establishes the proposed configuration's reliability and effectiveness through rigorous simulations and measurements using CST Microwave Studio, and vector network analyser (VNA). A comparative performance analysis underscores its suitability for sub-6 GHz 5G dual-band beamforming networks (BFNs), highlighting its compact size and improved band ratio as key advantages in advancing next-generation communication technologies.

REFERENCES

[1] A. C. Chen, "Advances in wireless communications technologies and their potential biomedical applications," in *Proc. IEEE Int. Conf. Inf. Technol. Appl. Biomed.*, May 1998, pp. 82–84.
[2] W. Rotman and R. Turner, "Wide-angle microwave lens for line source applications," *IEEE Trans. Antennas Propag.*, vol. AP-11, no. 6, pp. 623–632, Nov. 1963.
[3] J. Nolen, "Synthesis of multiple beam networks for arbitrary illumination," Ph.D. dissertation, Dept. Radio Division, Bendix Corp., Baltimore, MD, USA, 1965.
[4] J. Blass, "Multidirectional antenna—A new approach to stacked beams," *Proc. IRE Int. Conv. Rec.*, vol. 8, pp. 48–50, Mar. 1960.
[5] J. Butler and R. Lowe, "Beamforming matrix simplifies design of electrically scanned antennas," *Electron. Design*, vol. 9, no. 4, pp. 170–173, Apr. 1961.
[6] S. Nam, S. Choi, J. Ryu, and J. Lee, "Compact 28 GHz folded Butler matrix using low-temperature co-fired ceramics," *J. Electromagn. Eng. Sci.*, vol. 22, no. 4, pp. 452–458, Jul. 2022.
[7] J. Park and J. Kim, "A 28 GHz CMOS Butler matrix for 5G mm-wave beamforming systems," *Microwave Opt. Technol. Lett.*, vol. 62, no. 7, pp. 2499–2505, Jul. 2020.
[8] M. Wu, B. Zhang, Y. Zhou, and K. Huang, "A double-fold 7×8 Butler matrix-fed multibeam antenna with a boresight beam for 5G applications," *IEEE Antennas Wireless Propag. Lett.*, vol. 21, no. 3, pp. 516–520, Mar. 2022.
[9] Z.-P. Liu, F.-C. Chen, and C. Qin, "A 7×8 Butler matrix-fed multibeam antenna based on substrate integrated waveguide technology," *IEEE Antennas Wireless Propag. Lett.*, vol. 22, pp. 397–401, 2023, doi: 10.1109/LAWP.2022.3213786.
[10] K. Wincza, K. Staszek, I. Slomian, and S. Gruszczynski, "Scalable multibeam antenna arrays fed by dual-band modified Butler matrices," *IEEE Trans. Antennas Propag.*, vol. 64, no. 4, pp. 1287–1297, Apr. 2016.
[11] S. Zhu, Y. Ning, H. Chu, P. Xiao, and G. Li, "A low-profile dual-polarization programmable dual-beam scanning antenna array," *Frontiers Inf. Technol. Electron. Eng.*, vol. 24, no. 10, pp. 1504–1512, Oct. 2023.

[12] C. Collado, A. Grau, and F. De Flaviis, "Dual-band Butler matrix for WLAN systems," in *IEEE MTT-S Int. Microwave Symp. Dig.*, Jun. 2005, pp. 2247–2250.
[13] C. Zhou, J. Fu, H. Sun, and Q. Wu, "A novel compact dual-band Butler matrix design," in *Proc. 3rd Asia–Pacific Conf. Antennas Propag.*, Harbin, China, Jul. 2014, pp. 1327–1330.
[14] S. Zhou, Y. Liu, and Y. Wu, "Dual-band Butler matrix with the same phase difference for long-term evolution applications," *Electromagnetics*, vol. 36, no. 1, pp. 55–65, Jan. 2016.
[15] H. Ren, J. Shao, R. Zhou, B. Arigong, and H. Zhang, "Compact phased array antenna system based on dual-band operations," *Microwave Opt. Technol. Lett.*, vol. 56, no. 6, pp. 1391–1396, Jun. 2014.
[16] A. M. Zaidi, S. A. Imam, B. K. Kanaujia, K. Rambabu, K. Srivastava, and M. T. Beg, "A new dual band 4×4 Butler matrix with dual band 3 dB quadrature branch line coupler and dual band 45° phase shifter," *AEU Int. J. Electron. Commun.*, vol. 99, pp. 215–225, Feb. 2019.
[17] A. M. Zaidi, M. T. Beg, B. K. Kanaujia, J. Kishor, and K. Rambabu, "A novel dual band branch line coupler and its application to design a dual band 4×4 Butler matrix," *IEEE Access*, vol. 8, pp. 65104–65155, 2020.
[18] S.-S. Qi, Y. Guo, J. Wang, X. Wang, and W. Wu, "A dual-band filtering 4×4 Butler matrix based on SLR," *IEEE Antennas Wirel Propag. Lett.*, vol. 22, no. 12, pp. 3167–3171, Dec. 2023, doi: 10.1109/LAWP.2023.3312674.
[19] G. A. Adamidis, I. O. Vardiambasis, M. P. Ioannidou, and T. N. Kapetanakis, "Design and implentation od single-layer 4×4 and 8×8 Butler matrices for multibeam antenna arrays," *Int. J. Antennas Propag.*, vol. 2019, Mar. 2019, Art. no. 1645281, doi: 10.1155/2019/1645281.
[20] A. K. Vallappil, M. K. A. Rahim, B. A. Khawaja, N. A. Murad, and M. G. Mustapha, "Butler matrix based beamforming networks for phased array antenna systems: A comprehensive review and future directions for 5G applications," *IEEE Access*, vol. 9, pp. 3970–3987, 2021, doi: 10.1109/ACCESS.2020.3047696.
[21] A. B. Shallah, F. Zubir, M. K. A. Rahim, H. A. Majid, U. Ullah Sheikh, N. A. Murad, and Z. Yusoff, "Recent developments of Butler matrix from components design evolution to system integration for 5G beamforming applications: A survey," *IEEE Access*, vol. 10, pp. 88434–88456, 2022, doi: 10.1109/ACCESS.2022.3199739.
[22] A. Karimbu Vallappil, M. K. A. Rahim, B. A. Khawaja, and M. N. Iqbal, "Compact metamaterial based 4×4 Butler matrix with improved bandwidth for 5G applications," *IEEE Access*, vol. 8, pp. 13573–13583, 2020, doi: 10.1109/ACCESS.2020.2966125.
[23] A. S. Mohra, "Dual band branch-line coupler using T and Π sections," in *Proc. 4th Int. Conf. New Paradigm Electron. Inf. Technol.*, Jun. 2016, pp. 1–7.
[24] A. B. Shallah, F. Zubir, M. K. A. Rahim, A. Abubakar, Z. Yusoff, and M. Aminu-Baba, "A miniaturized branch line coupler for 5G dual band applications," in *Proc. Int. Symp. Antennas Propag. (ISAP)*, Oct. 2022, pp. 513–514.
[25] S. Singh, R. P. Yadav, and A. Jain, "Miniaturized dual-band branch-line coupler with folded stubs," in *Proc. IEEE 5th Int. Conf. Converg. Technol. (I2CT)*, Mar. 2019, pp. 1–4.
[26] A. Chakraborty Das, L. Murmu, and S. Dwari, "A compact branch-line coupler using folded microstrip lines," in *Proc. Int. Conf. Microwave Photon. (ICMAP)*, Dec. 2013, pp. 1–3.
[27] A. B. Shallah, F. Zubir, M. K. A. Rahim, M. R. Hamid, A. K. Vallappil, H. A. Majid, Z. Yusoff, and A. Basit, "A compact metamaterial dual-band branch-line coupler for 5G applications," *ELEKTRIKA- J. Electr. Eng.*, vol. 22, no. 2, pp. 30–36, Aug. 2023.
[28] A. K. Vallappil, M. K. A. Rahim, B. A. Khawaja, and M. Aminu-Baba, "Metamaterial based compact branch-line coupler with enhanced bandwidth for use in 5G applications," *Appl. Comput. Electromagn. Soc. J.*, vol. 35, no. 5, pp. 700–708, Jun. 2020.
[29] S. Sahin, N. K. Nahar, and K. Sertel, "A simplified Nicolson–Ross–Weir method for material characterization using single-port measurements," *IEEE Trans. Terahertz Sci. Technol.*, vol. 10, no. 4, pp. 404–410, Jul. 2020, doi: 10.1109/TTHZ.2020.2980442.
[30] J. Shao, H. Ren, B. Arigong, C. Li, and H. Zhang, "A fully symmetrical crossover and its dual-frequency application," *IEEE Trans. Microwave Theory Techn.*, vol. 60, no. 8, pp. 2410–2416, Aug. 2012.
[31] A. B. Shallah, F. Zubir, and M. K. A. Rahim, "A metamaterial-based dual-band ±45° phase shifter for 5G lower band applications," in *Proc. IEEE Int. Symp. Antennas Propag. (ISAP)*, Malaysia, Oct. 2023, pp. 1–2.
[32] J. Yan, X. Liu, C. Ma, Y. Huang, and G. Yang, "All-dielectric materials and related nanophotonic applications," *Mater. Sci. Eng. R, Rep.*, vol. 141, Jul. 2020, Art. no. 100563.
[33] Y. Wang, K. Ma, and Z. Jian, "A low-loss Butler matrix using patch element and honeycomb concept on SISL platform," *IEEE Trans. Microwave Theory Techn.*, vol. 66, no. 8, pp. 3622–3631, Aug. 2018.
[34] H. Ren, *Design and Application of Phased Array System*. Dallas, TX, USA: University of North Texas, 2013.
[35] C. A. Balanis, *Antenna Theory: Analysis and Design*. Hoboken, NJ, USA: Wiley, 2016.
[36] R. Sunitha, S. Vijayanand, R. Kannan, S. Usha, L. Rangaiah, and P. Sanjay, "Butler matrix design and simulation for 5G applications," in *Proc. Int. Conf. Future Trends Smart Communities (ICFTSC)*, Dec. 2022, pp. 33–38.
[37] A. K. Vallappil, M. Kamal A. Rahim, B. A. Khawaja, and M. N. Iqbal, "A miniaturized metamaterial-loaded switched-beam antenna array system with enhanced bandwidth for 5G applications," *IEEE Access*, vol. 12, pp. 6684–6697, 2024, doi: 10.1109/ACCESS.2024.3351475.
[38] Q. Wu, J. Jing, X.-W. Zhu, and C. Yu, "Digital predistortion for concurrent dual-band millimeter wave analog multibeam transmitters," *IEEE Trans. Circuits Syst. II, Exp. Briefs*, vol. 69, no. 3, pp. 1747–1751, Mar. 2022, doi: 10.1109/TCSII.2021.3105301.

ABDULKADIR BELLO SHALLAH (Member, IEEE) was born in Gwandu, Kebbi State, Nigeria, in 1984. He received the B.Eng. degree in electrical and electronics engineering from Bayero University, Kano, in 2014, and the M.Eng. degree in electronics and telecommunications from Universiti Teknologi Malaysia, in 2017, where he is currently pursuing the Ph.D. with the Faculty of Electrical Engineering. He has been a Lecturer with the Electrical and Electronics Engineering Department, Faculty of Engineering, Kebbi State University of Science and Technology, Aliero, Kebbi State. His research interests include RF and microwave devices, reflectarray antenna, beamforming networks, and metamaterials.

FARID ZUBIR (Member, IEEE) received the B.Eng. degree in electrical, majoring in telecommunication, and the M.Eng. degree in RF and microwave from Universiti Teknologi Malaysia (UTM), in 2008 and 2010, respectively, and the Ph.D. degree from the University of Birmingham, U.K., in 2016, for research into direct integration of power amplifiers with antennas in microwave transmitters. He is currently an Assistant Professor with the Department of Communication Engineering, Faculty of Electrical Engineering, UTM. In 2019, he was an Honorary Postdoctoral Research Fellow for two years with The University of British Columbia (UBCO), Okanagan, Canada, where he conducted research into highly efficient and linear amplification power amplifier topology for wireless power systems. His research interests include RF and microwave technologies, including planar array antennas, dielectric resonator antennas (DRA), and active integrated antennas (AIA).

MOHAMAD KAMAL A. RAHIM (Senior Member, IEEE) was born in Alor Setar, Malaysia, in 1964. He received the B.Eng. degree in electrical and electronic engineering from the University of Strathclyde, U.K., in 1987, the master's degree in engineering from the University of New South Wales, Australia, in 1992, and the Ph.D. degree in wideband active antenna from the University of Birmingham, U.K., in 2003. From 1992 to 1999, he was a Lecturer with the Faculty of Electrical Engineering, Universiti Teknologi Malaysia, where he was a Senior Lecturer with the Department of Communication Engineering, from 2005 to 2007, and he is currently a Professor. His research interests include the design of active and passive antennas, dielectric resonator antennas, microstrip antennas, reflectarray antennas, electromagnetic bandgaps, artificial magnetic conductors, left-handed metamaterials, and computer-aided design for antennas.

NOORLINDAWATY MD. JIZAT (Member, IEEE) received the B.E. and M.S. degrees in electrical engineering (telecommunication) from Universiti Teknologi Malaysia (UTM), Skudai, in 2008 and 2010, respectively. She is currently pursuing the Ph.D. degree in electrical engineering (telecommunication) with Multimedia University (MMU), Malaysia. From 2008 to 2012, she was a Quality Engineer with Flextronics Technology Sdn Bhd and a Research and Development (R & D) Engineer with Panasonic System Network Malaysia. She is also a Lecturer with the Faculty of Engineering, MMU. Her research interests include beamforming networks, butler matrix, beam steering, antenna arrays, self-powered solar Wi-Fi systems, and material research into antenna applications.

ABDUL BASIT received the B.Sc. degree in electrical engineering from the University of Engineering and Technology Peshawar, Pakistan, in 2012, the M.Sc. degree from the CECOS University of IT and Emerging Sciences Peshawar, Pakistan, in 2015, and the Ph.D. degree in electrical engineering from the University of Engineering and Technology Peshawar, in 2021. From 2013 to 2017, he was a Lecturer with the Department of Electrical Engineering, University of Engineering and Technology Bannu Campus, Pakistan. From 2017 to 2018, he was an Assistant Director (Technical) with National Transmission and Dispatch Company (NTDC), Pakistan. He is currently a Postdoctoral Scientific Researcher with Ningbo Institute of Technology, Zhejiang University, China. His research interests include the design of microwave filters, power-integrated differential controllers, antenna design at millimeter-wave, and terahertz applications.

MAHER ASSAAD received the master's degree in electrical engineering/microelectronics IC design from the University of Montreal, Montreal, Canada, in 2002, and the Ph.D. degree in electrical engineering/microelectronics IC design from the University of Glasgow, Glasgow, U.K., in 2009. He was a Senior Electrical Engineering Lecturer with Universiti Teknologi PETRONAS, Malaysia, and an Associate Professor in electronic and communication engineering with American University of Ras Al Khaimah, United Arab Emirates. He is currently a Professor in electrical and computer engineering with Ajman University, United Arab Emirates. His research interests include the design of circuits/integrated circuits for various types of sensors and wireline and optical communication systems.

HUDA A. MAJID (Member, IEEE) received the B.Eng. degree in electrical engineering (telecommunication) and the M.Eng. and Ph.D. degrees in electrical engineering from Universiti Teknologi Malaysia (UTM), in 2007, 2010, and 2013, respectively. He is currently an Associate Professor and the Head of the Emerging Telecommunication Technology Focus Group, Department of Electrical Engineering Technology, Faculty of Engineering Technology, Universiti Tun Hussein Onn Malaysia (UTHM) Pagoh Kampus, Johor Darul Ta'zim. Before joining UTHM, he was a Postdoctoral Fellow with UTM for one year. He scores an H-index of 21 (SCOPUS index) and he has led a few grants under the Ministry of Higher Education Malaysia and Industrial Grants worth more than RM200k. He has published more than 100 international journals and paper conferences. His research interests include planar and flexible antennas, array antennas, reconfigurable antennas, metamaterial, RF microwave devices, and the IoT applications.